Supporting Information

Spatio-temporal tracking the transporting of RNA nano-drugs: from transmembrane to intracellular delivery

Xuelei Pang[a], Qingrong Zhang [a], Siying Li,[a] Jing Zhao[a], Mingjun Cai[b], Hongda Wang[b], Haijiao Xu[b], Guocheng Yang[a], and Yuping Shan*[a]

[a] School of Chemistry and Life Science, Advanced Institute of Materials Science, Changchun University of Technology, Changchun 130012, China.

[b] Changchun Institute of Applied Chemistry, State Key Laboratory of Electroanalytical Chemistry, Chinese Academy of Science, Changchun 130022, China.

* Corresponding authors: Yuping Shan (shanyp@ ciac.ac.cn)

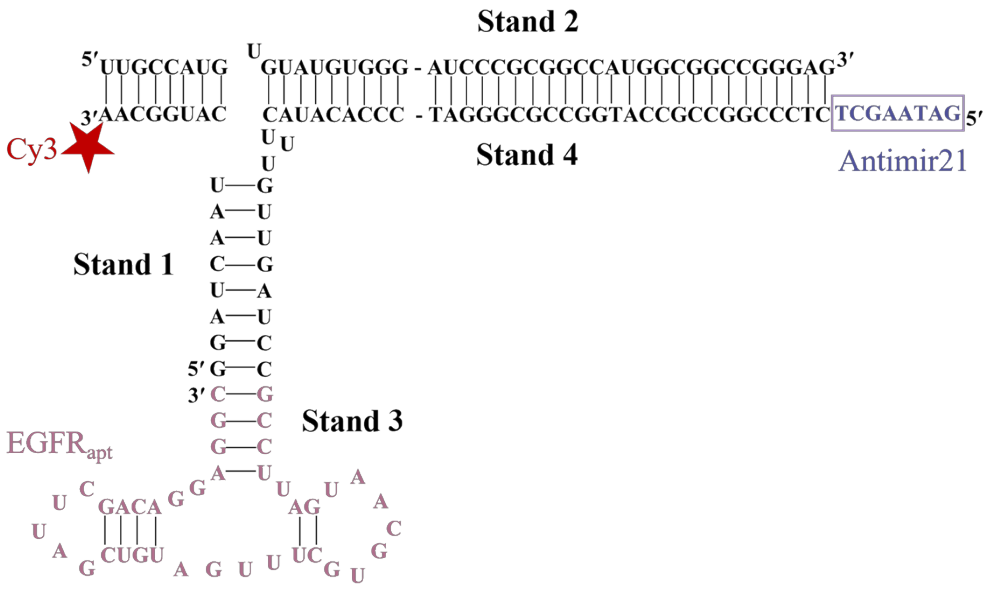

Fig. S1 2D sequence of the Antimir21-RNP-Apt.

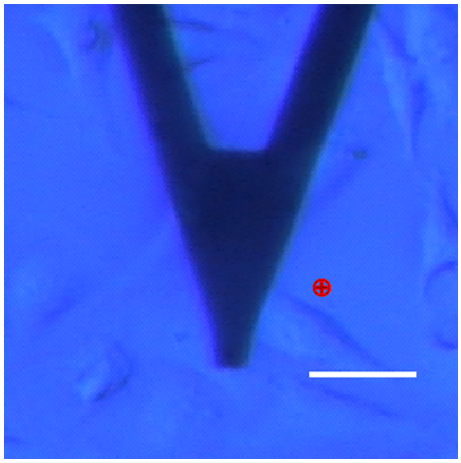

Fig. S2 Optical image of AFM tip cantilever above living MDA-MB-231 cells. (Scale bar: 60 μm).

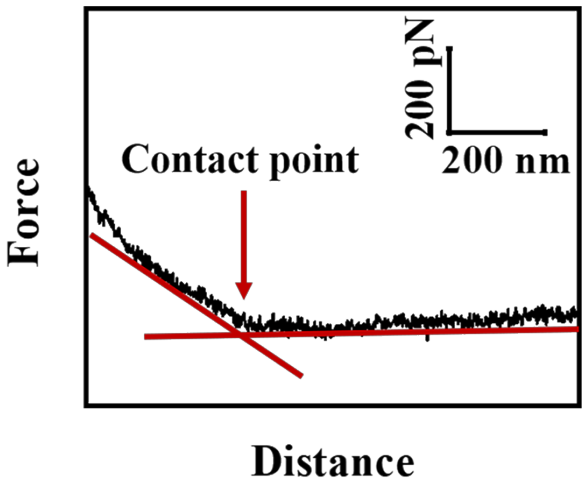

Fig. S3 Engaging the RNPs modified AFM tip onto the cell membrane to find the contact point where the AFM tip contacts the cell membrane. The contact point is the intersection of the flat part and the slope (red line) of the force-distance curve.

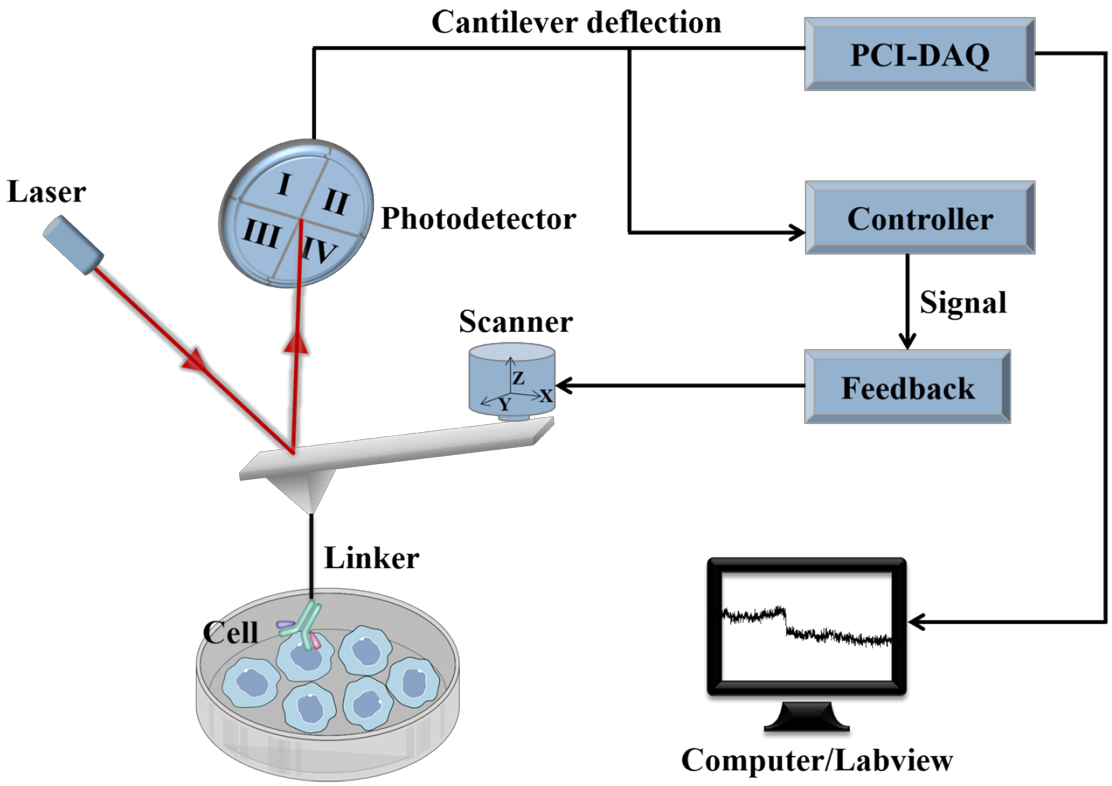

Fig. S4 Schematic diagram of force tracing technique workflow. The laser beam is reflected by the AFM tip cantilever and directed toward the photodetector. The deflection of the AFM tip cantilever will be recorded and converted into force-time curves by PCI-DAQ controlled with LabVIEW. The sampling rate of the data acquisition is 2MS s^{-1}, and a 100 HZ low-pass filter is used to eliminate high-frequency noise in electronic equipment and the environment.

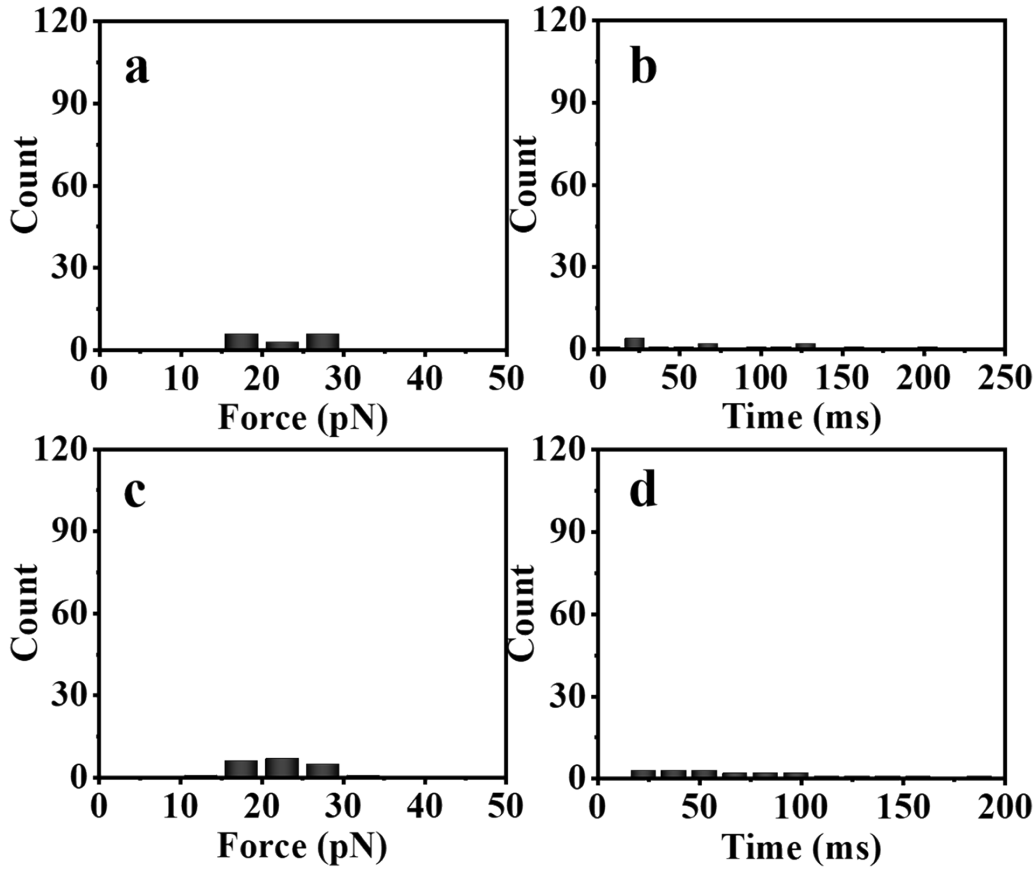

Fig. S5 Control experiments. (a,b) The force and duration distribution of force-time curves performed by unmodified AFM tip (clean tip) on MDA-MB-231cell surface. (c,d) The force and duration distribution of force-time curves performed by PEG linker modified AFM tip on MDA-MB-231cell surface.

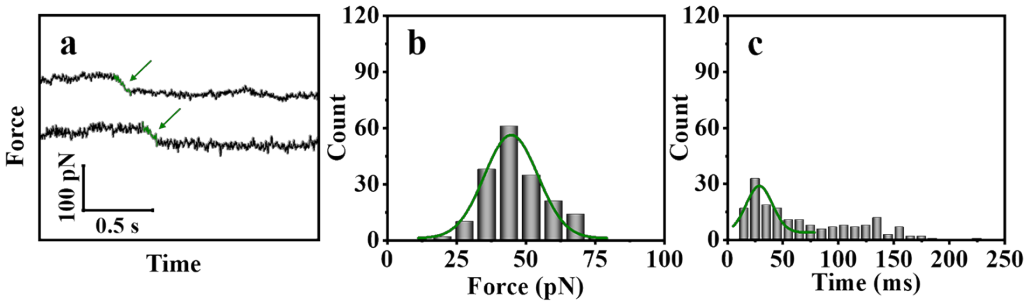

Fig. S6 The dynamic parameters of single Antimir21-RNP-MUT entry MDA-MB-231 cell detected by force tracing. (a) Typical force-time curves for Antimir21-RNP-MUT internalization, the green parts indicate the cell entry process. (b) The histogram of Antimir21-RNP-MUT endocytic force. (c) The duration distribution for Antimir21-RNP-MUT endocytosis.

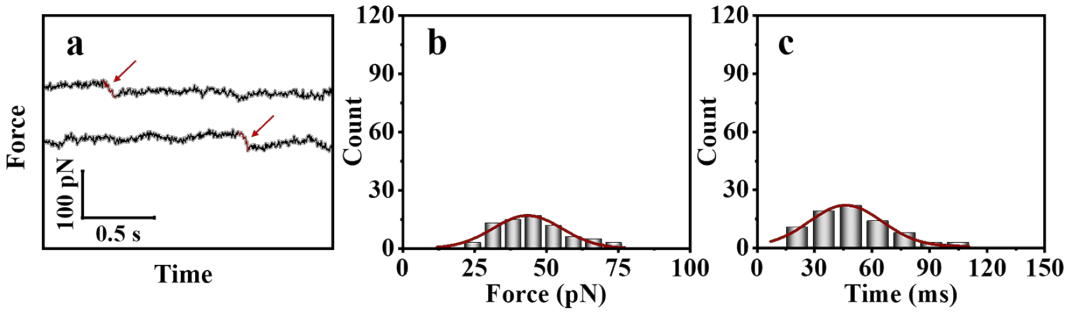

Fig. S7 The force and duration distribution for Antimir21-RNP-Apt entry HEK-293 cell measured by force tracing. (a) The typical force-time curves for Antimir21-RNP-Apt internalization entry into HEK-293 cell, the red parts indicate the cell entry process. (b) The histogram of endocytic force of Antimir21-RNP-Apt entry HEK-293 cell. (c) The duration distribution for Antimir21-RNP-Apt entry HEK-293 cell.

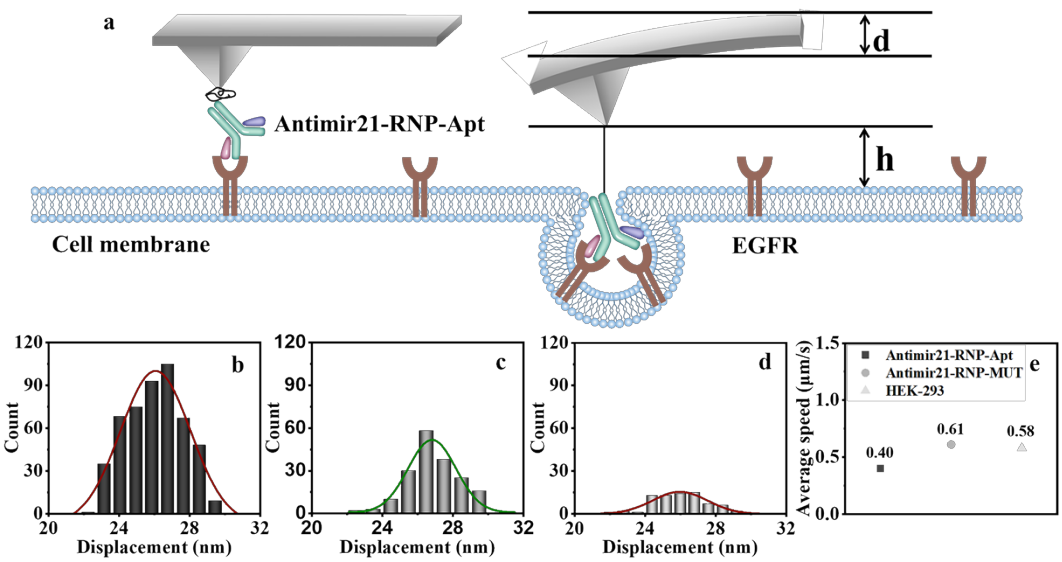

Fig. S8 The displacement during the process of RNPs entry cells. (a) The schematic of displacement during the process of RNPs entry the living cells. The displacement is composed of the bending distance *d* of the AFM tip cantilever and the extension length *h* of the PEG linker. (b) The displacement distribution for Antimir21-RNP-Apt entry MDA-MB-231 cell, which is in the range of 22.5-29.7 nm with an average value of 26.0±1.6 nm. (N≈500). (c) The displacement distribution for Antimir21-RNP-MUT entry MDA-MB-231 cell, which is in the range of 22.7-29.9 nm with an average value of 26.9±1.5 nm. (N≈200). (d) The displacement distribution for Antimir21-RNP-Apt entry HEK-293 cell, which is in the range of 22.1-28.9 nm with an average value of 26.0±1.5 nm. (N≈100). (e) The average speed for Antimir21-RNP-Apt entry MDA-MB-231 cell, Antimir21-RNP-MUT entry MDA-MB-231 cell, and Antimir21-RNP-Apt entry HEK-293 cell.

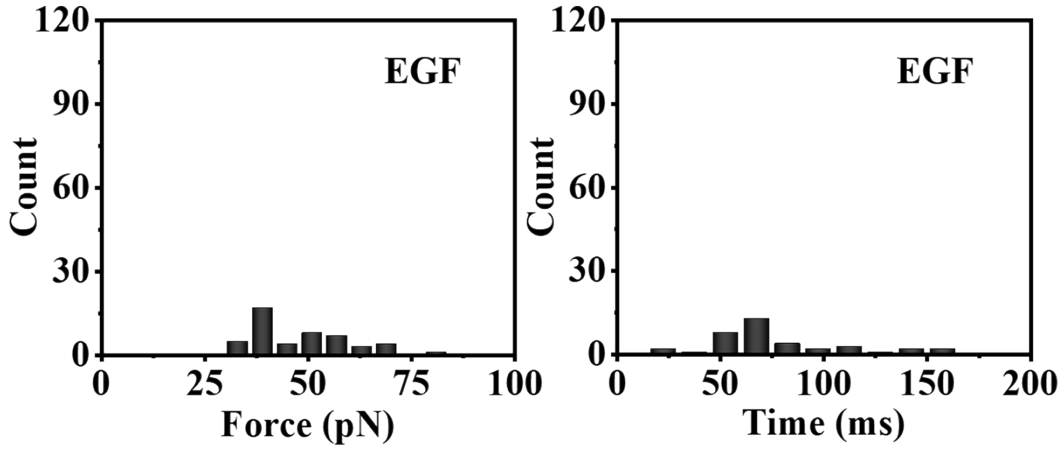

Fig. S9 The distribution of force and duration for Antimir21-RNP-Apt entry MDA-MB-231 cells after blocking with EGF.

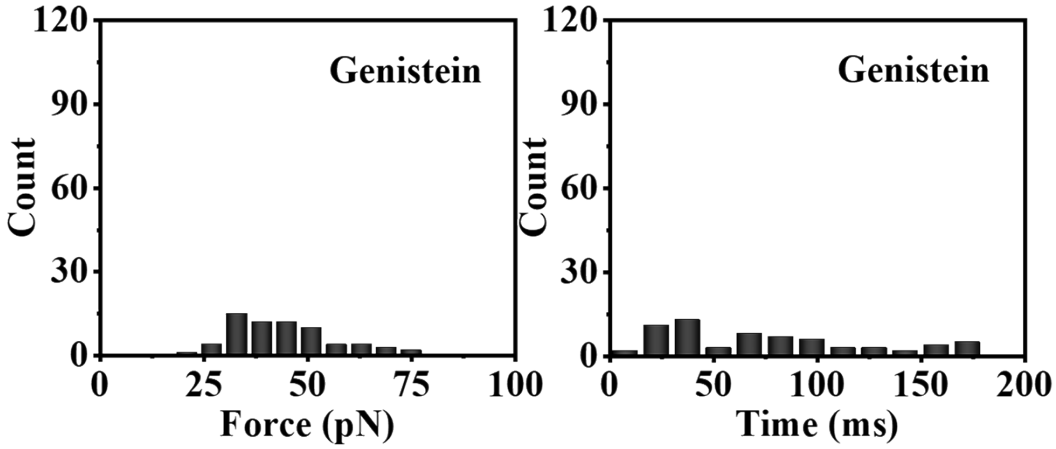

Fig. S10 The distribution of force and duration for Antimir21-RNP-Apt entry MDA-MB-231 cells after blocking with genistein.

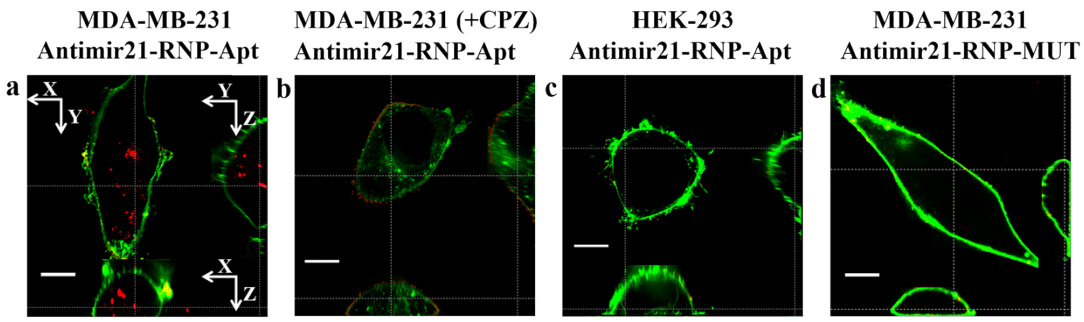

Fig. S11 The magnified XY plane and XZ cross-section images of Antimir21-RNP-Apt in cells. (a) The fluorescence image of MDA-MB-231 cells after incubation with Antimir21-RNP-Apt. (b) The fluorescence image of CPZ pretreated MDA-MB-231 cells after incubation with Antimir21-RNP-Apt. (c) The fluorescence image of HEK-293 cell after incubation with Antimir21-RNP-Apt. (d) The fluorescence image of MDA-MB-231 cells after incubation with Antimir21-RNP-MUT.

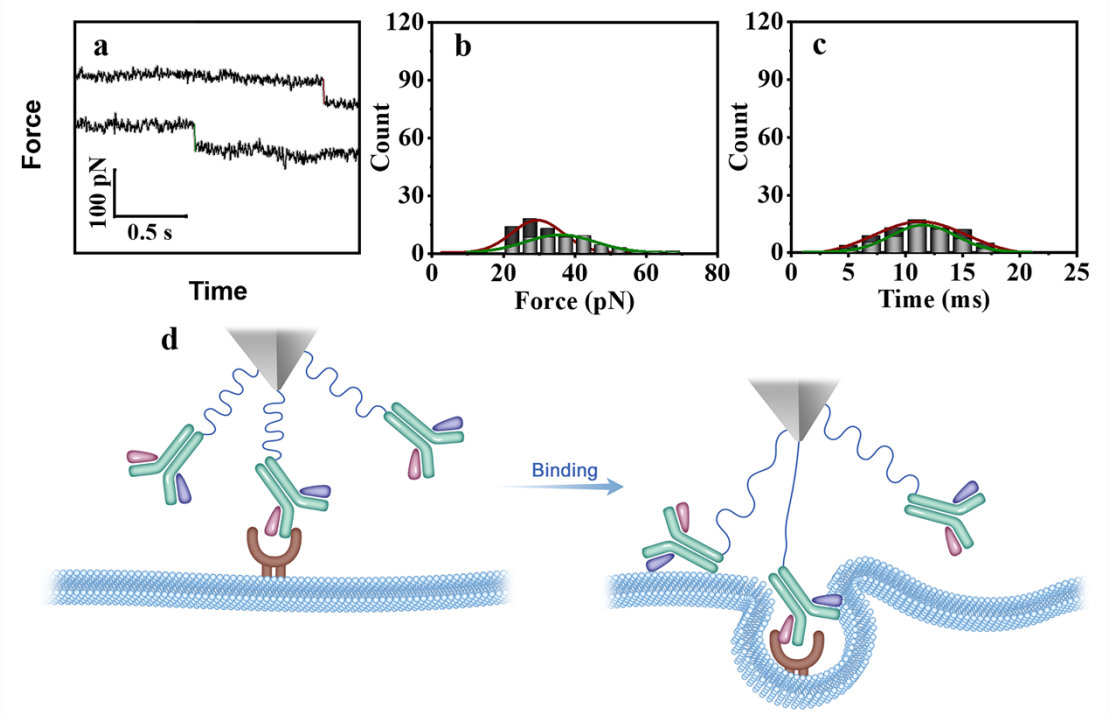

Fig. S12 Analysis the binding of Antimir21-RNP-Apt and Antimir21-RNP-MUT with cell membrane. (a) Typical force-time curves for RNPs binding with cell membrane, Antimir21-RNP-Apt (red section) and Antimir21-RNP-MUT (green section) binding with cell membrane. (b) Distribution of the binding force for Antimir21-RNP-Apt (red) and Antimir21-RNP-MUT (green). (c) Distribution of the time for Antimir21-RNP-Apt (red) and Antimir21-RNP-MUT (green) binding with cell membrane. (d) Schematic diagram of the RNPs binding to cell membrane during the internalization process.

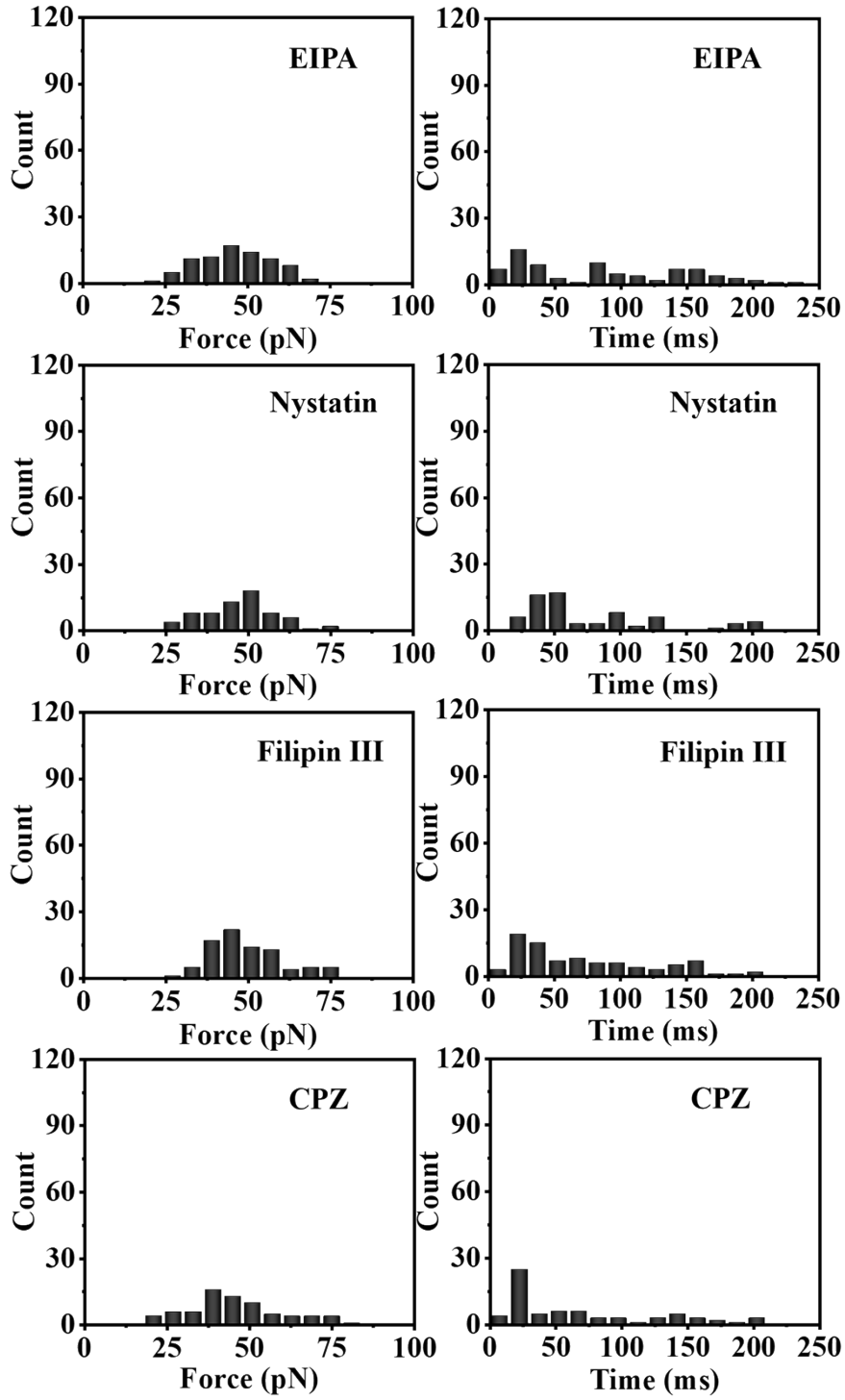

Fig. S13 Blocking experiments. Force and duration distribution for Antimir21-RNP-Apt entry MDA-MB-231 cells after blocking with EIPA, nystatin, Filipin III, and CPZ.

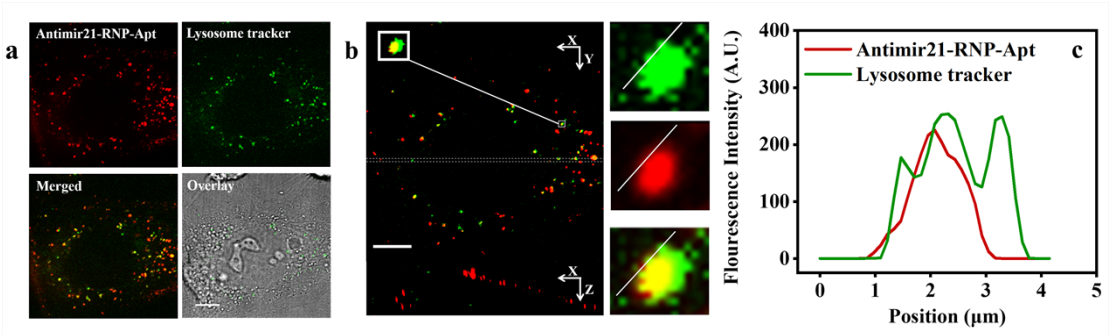

Fig. S14 Colocalization of Antimir21-RNP-Apt with lysosomes. (a) Confocal images of Antimir21-RNP-Apt and lysosomes. The scale bar is 10 μm. (b) The magnified XY plane and XZ cross-section plane of a. The scale bar is 10 μm. (c) Fluorescence intensity profile of lysosomes (green) and Antimir21-RNP-Apt (red) corresponding to the green and red particles marked with white lines in right panel of b.

Table S1. Summary the dynamic parameters of RNPs entry cell as measured by force tracing technique. Dynamic parameters for Antimir21-RNP-Apt entry MDA-MB-231 cells, Antimir21-RNP-MUT entry MDA-MB-231 cells, and Antimir21-RNP-Apt entry HEK-293 cells.

	Force (pN)	Time (ms)	Speed (um/s)	Displacement (nm)	Probability (%)
Antimir21-RNP-Apt (MDA-MB-231)	46±12	81.9±39.8	0.40±0.19	26.0±1.6	18.3
Antimir21-RNP-MUT (MDA-MB-231)	47±11	69.5±47.2	0.61±0.40	26.9±1.5	3.8
Antimir21-RNP-Apt (HEK-293)	45±12	50.8±20.8	0.58±0.40	26.0±1.5	3.6